J. Am. Chem. Soc. **1997,** *119,* 4021−4032

4021

Ab Initio Molecular Orbital Theory on Intramolecular Charge Polarization: Effect of Hydrogen Abstraction on the Charge Sensitivity of Aromatic and Nonaromatic Species

Akihiro Morita and Shigeki Kato*

Contribution from the Department of Chemistry, Graduate School of Science, Kyoto University, Kitashirakawa, Sakyo-ku, Kyoto 606, Japan

Received October 9, 1996. Revised Manuscript Received December 31, 1996[⊗]

Abstract: We performed *ab initio* molecular orbital (MO) calculations of the response kernel $(\partial Q_a/\partial V_b)$, which represents the response of the intramolecular charge polarization by external electrostatic field, on the basis of the coupled perturbed Hartree−Fock equation. The response kernels of some organic molecules including pyrazine, pyrazinyl radical, acetone, and 2-hydroxypropyl radical were calculated along the present formulation. The results revealed that the hydrogen abstraction of pyrazine causes the product radical to be remarkably deformable in the partial charge distribution, while the hydrogen abstraction of acetone does not induce such enhancement of the charge sensitivity. The augmented sensitivity does not appear in the usual polarizability for a uniform field but emerges for a local fluctuated field. To elucidate the remarkable difference, we performed the normal mode analysis and decomposition based on the intrinsic soft MO pairs or localized orbitals. As a result, the enhancement in the aromatic species is attributed to the softest normal mode due to the $\pi-\sigma$ mixing that facilitates the deformation of the π-electron orbitals. In the nonaromatic species, on the other hand, this effect is not dominant and is canceled by the breakdown of hyperconjugation. We suggest that the particular sensitivity of aromatic radicals is the origin of anomalously slow diffusion in solution.

1. Introduction

Electronic structure of a molecule generally deviates from that in the isolated environment due to the existence of neighboring molecules, *e.g.* a reaction partner during the course of reaction or solvent molecules in solution. Detailed understanding of the distorted electronic structure is thus indispensable when we elucidate reactivity or solvent effect in solution, but the understanding is far from complete at present. One of the promising ways to represent the deformed electronic structure is to utilize the partial charge distribution assigned to the constituent atoms. This approach is suitable to deal with the intermolecular interaction, since the charge distribution governs the electrostatic force.

In the present paper, we propose a method to calculate directly the response kernel $(\partial Q_a/\partial V_b)_N$, where Q_a denotes the partial charge at the site a and V_b the electrostatic potential at the site b. The suffix N denoting the number of total electrons of the molecule indicates that the derivative is taken under the constant electron number. This is a basic quantity to describe the response of intramolecular charge polarization induced by the external electrostatic field. We defined this quantity with accommodating it to the *ab initio* molecular orbital (MO) theory and calculated it via the coupled perturbed Hartree−Fock (CPHF) equation[1−3] of restricted Hartree−Fock (RHF) and unrestricted Hartree−Fock (UHF) wave functions.

The concept of the response kernel was originally introduced in the density functional theory to express the electron redistribution[4] as

$$\left(\frac{\delta\rho(\boldsymbol{r})}{\delta\upsilon(\boldsymbol{r}')}\right)_N = \frac{\delta^2 E}{\delta\upsilon(\boldsymbol{r})\,\delta\upsilon(\boldsymbol{r}')} \tag{1}$$

Our expression of the response kernel $(\partial Q_a/\partial V_b)_N$ is considered to be a coarse-grained version based on the site representation, while treated from the viewpoint of the *ab initio* MO theory. In the density functional theory, the flow of electrons is rigorously formulated via the electronegativity equalization principle,[5−8] which made an essential basis of the charge sensitivity analysis to study the response by the populational or electrostatic perturbation.[9−15] Recently there have been reported some seminal attempts to apply this approach to molecular simulation[16−18] in order to incorporate the polarization effect into the intermolecular interaction. This approach has conceptually a sound basis and certainly rich potential to shed light on the chemical problems. However, in our opinion, the progress has been hindered by a shortage of reliable numerical

⊗ Abstract published in *Advance ACS Abstracts,* April 15, 1997.

(1) (a) Gerratt, J.; Mills, I. M. *J. Chem. Phys.* **1968**, *49*, 1719. (b) *Ibid.* **1968**, *49*, 1730.

(2) Pople, J. A.; Krishnan, R.; Schlegel, H. B.; Binkley, J. S. *Int. J. Quantum Chem. Symp.* **1979**, *13*, 225.

(3) Pulay, P. *Adv. Chem. Phys.* **1987**, *69*, 241.

(4) Parr, R. G.; Yang, W. *Density-Functional Theory of Atoms and Molecules*; Oxford Univ.: New York, 1989.

(5) Sanderson, R. T. *Science* **1951**, *114*, 670.

(6) Mortier, W. J.; van Genechten, K.; Gasteiger, J. *J. Am. Chem. Soc.* **1985**, *107*, 829.

(7) Mortier, W. J.; Ghosh, S. K.; Shankar, S. *J. Chem. Phys.* **1987**, *86*, 5063.

(8) Baekelandt, B. G.; Mortier, W. J.; Schoonheydt, R. A. In *Chemical Hardness*; Springer-Verlag: Berlin, 1993; Vol. 80 of *Structure and Bonding*, p 187.

(9) Nalewajski, R. F. In *Chemical Hardness*; Springer-Verlag: Berlin, 1993; Vol. 80 of *Structure and Bonding*, p 115.

(10) Nalewajski, R. F.; Korchowiec, J.; Zhou, Z. *Int. J. Quantum Chem. Symp.* **1988**, *22*, 349.

(11) (a) Ghanty, T. K.; Ghosh, S. K. *J. Phys. Chem.* **1991**, *95*, 6512. (b) *Ibid.* **1994**, *98*, 1840.

(12) Ghanty, T. K.; Ghosh, S. K. *J. Am. Chem. Soc.* **1994**, *116*, 3943.

(13) Korchowiec, J.; Nalewajski, R. F. *Int. J. Quantum Chem.* **1992**, *44*, 1027.

(14) Baekelandt, B. G.; Mortier, W. J.; Lievens, J. L.; Schoonheydt, R. A. *J. Am. Chem. Soc.* **1991**, *113*, 6730.

(15) Nalewajski, R. F.; Korchowiec, J. *J. Mol. Catal.* **1991**, *68*, 123.

(16) Rappe, A. K.; Goddard, W. A., III. *J. Phys. Chem.* **1991**, *95*, 3358.

(17) Rick, S.; Stuart, S. J.; Berne, B. J. *J. Chem. Phys.* **1994**, *101*, 6141.

(18) York, D. M.; Yang, W. *J. Chem. Phys.* **1996**, *104*, 159.

methods; most of the numerical results so far of the charge sensitivity analysis involve crude approximation with empirical parameters. Our method would provide a useful means to calculate the response kernel via the *ab initio* MO theory.

The deformation of the electronic structure is considered to be the origin of the many-body interaction via the "polarizability effect", which has been drawing great attention in the condensed phase chemistry.[19] To examine the effect by molecular simulation, the intramolecular polarization was usually modeled with the phenomenological site-polarizable model.[20-28] This model has both permanent partial charges and polarizabilities at some sites of the molecule to describe the polar interaction. It is evident that the interaction site model with the response kernel is also capable of incorporating the polarizability effect in another way by considering the redistribution of the partial charges. We think that our model has some advantages over the site-polarizable model to be implemented to the molecular simulation. First, our model is free from ambiguities to define the site polarizability, since employing atomic polarizability as the site polarizability is highly questionable under a molecular environment.[29] The redistributed charges in our model are automatically determined to reproduce the surrounding electrostatic field via the least square fitting. The present model is applicable to any molecule that is capable of *ab initio* MO calculations, and no further fitting procedure is necessary. Second, the present model can well describe correlation of polarization among the different sites. It is particularly important to consider the response of delocalized π-electrons, since the response is not restricted to a local site. The correlated response of polarization shows a variety of patterns with various molecules, reflecting their electronic structures. Such characteristic correlation is beyond the description by classical electrostatic response at each site.

We calculated the response kernels of pyrazine, pyrazinyl radical, acetone, and 2-hydroxypropyl radical as well as benzene and β-propyl radical. Our choice of systems was motivated by a recent experimental finding made by Terazima et al.[30] They measured the diffusion coefficients of various radicals using the transient grating technique,[31] which enabled us to evaluate the diffusion of short-lived, low-concentrated species. They found that some π-radicals, including pyrazinyl radical or benzophenone ketyl radical, show 2−4 times slower diffusion than the corresponding parents, pyrazine or benzophenone, while some σ-radicals like 2-hydroxypropyl radical do not show much difference in diffusion coefficient from that of the parent, acetone or 2-propanol. The result was surprising, since the radical species is formed by adding only one hydrogen atom to the corresponding parent molecule. That difference does not seem to make a significant difference in molecular size or

interaction. The excessive slow diffusion of the radicals implies an unknown radical−solvent interaction, but the origin has not been identified yet. To elucidate it theoretically, we investigated the electronic structure of the radicals and parents by considering possible electronic distortion in solution. Further calculations of molecular dynamics simulation to evaluate the diffusion coefficients will be reported in a future paper.

The remainder of this paper is constructed as follows. The next section describes the theoretical methods used to calculate the response kernel and further analysis based on the normal modes and the intrinsic MO pairs. We then present the results of the response kernel and the analysis of the above-mentioned species in section 3 and elucidate the remarkably different influence of the hydrogen abstraction on the charge sensitivity. The conclusions are followed in section 4.

2. Theoretical Methods

2.1. Response Kernel. 2.1.1. Definition. We first give a rigorous expression of the response kernel $(\partial Q_a/\partial V_b)_N$ in the *ab initio* MO theory, where Q_a is the partial charge at the site a and V_b the electrostatic potential at the site b. The perturbation by surrounding media is represented using the electrostatic external potential V_a acting at each site a. The choice of the sites is arbitrary, but they are usually taken to be all (or some) atomic positions of the molecule. The perturbation Hamiltonian to the electronic state $\hat{H}'$ is given as

$$\hat{H}' = \sum_a^{\text{site}} e(-\hat{N}_a + Z_a)V_a \qquad (2)$$

where $\hat{N}_a$ denotes the electronic number operator at the site a and Z_a is the nuclear charge. The electronic occupation number at the site a, N_a, is expressed as

$$N_a = \langle\Psi|\hat{N}_a|\Psi\rangle = \sum_{p,q}^{\text{AO}} D_{pq}\langle p|\hat{n}_a|q\rangle \qquad (3)$$

Ψ and D_{pq} denote the electronic wave function and one-electron density matrix, respectively. $\hat{n}_a$ is the number operator for a single electron, the sum of which constitutes the total operator $\hat{N}_a = \sum_i^{\text{electron}} n_a(i)$. The electronic occupation number N_a is determined by the standard least-square-fitting procedure to the electrostatic potential originated by the electrons of the molecule, which is evaluated at some spatial grid points around the molecule. The sum of the square deviation L,

$$L = \sum_n^{\text{grid}} w_n \left(\sum_{p,q}^{\text{AO}} D_{pq} \left\langle p \left| \frac{1}{|\boldsymbol{r} - \boldsymbol{R}_G(n)|} \right| q \right\rangle - \sum_a^{\text{site}} \frac{N_a}{|\boldsymbol{R}_s(a) - \boldsymbol{R}_G(n)|} \right)^2 \qquad (4)$$

is the subject to be minimized under the conservation of total electron number N. $\boldsymbol{R}_G(n)$, $\boldsymbol{R}_s(a)$, and $\boldsymbol{r}$ denote the coordinates of nth grid point, ath site, and electron, respectively. w_n is the weight factor of the nth grid point. The equation to be solved is

$$\frac{\partial}{\partial N_a}\left[L - \lambda\left(\sum_b^{\text{site}} N_b - N\right)\right] = 0 \qquad (5)$$

where λ is the Lagrange multiplier. The resultant value of N_a is given as follows:

$$N_a = \sum_{p,q}^{\text{AO}} D_{pq}\langle p|\hat{n}_a|q\rangle$$

$$= \sum_{p,q}^{\text{AO}} D_{pq}\left\langle p \left| \sum_b^{\text{site}}(A^{-1})_{ab}\left\{ B_b + \frac{1 - \sum_{c,d}^{\text{site}}(A^{-1})_{cd}B_c}{\sum_{c,d}^{\text{site}}(A^{-1})_{cd}} \right\} \right| q \right\rangle \qquad (6)$$

where

(19) Elrod, M. J.; Saykally, R. J. *Chem. Rev.* **1994**, *94*, 1975.

(20) Ahlström, P.; Wallqvist, A.; Engström, S.; Jönsson, B. *Mol. Phys.* **1989**, *68*, 563.

(21) Neesar, U.; Corongiu, G.; Clementi, E.; Kneller, G. R.; Bhattacharya, D. K. *J. Phys. Chem.* **1990**, *94*, 7949.

(22) Sprik, M. *J. Phys. Chem.* **1991**, *95*, 2283.

(23) Sprik, M.; Klein, M. L. *J. Chem. Phys.* **1988**, *89*, 7556.

(24) Rullmann, J. A. C.; van Duijnen, P. T. *Mol. Phys.* **1988**, *63*, 451.

(25) Walqvist, A.; Ahlström, P.; Karlström, G. *J. Phys. Chem.* **1990**, *94*, 1649.

(26) van Belle, D.; Froeyen, M.; Lippens, G.; Wodak, S. J. *Mol. Phys.* **1992**, *77*, 239.

(27) Bernardo, D. N.; Ding, Y.; K.-Jespersen, K.; Levy, R. M. *J. Phys. Chem.* **1994**, *98*, 4180.

(28) Caldwell, J.; Dang, L. X.; Kollman, P. A. *J. Am. Chem. Soc.* **1990**, *112*, 9144.

(29) Miller, K. J. *J. Am. Chem. Soc.* **1990**, *112*, 8543.

(30) (a) Terazima, M.; Okamoto, K.; Hirota, N. *J. Chem. Phys.* **1995**, *102*, 2506. (b) Terazima, M.; Okamoto, K.; Hirota, N. *J. Phys. Chem.* **1993**, *97*, 13387.

(31) Terazima, M.; Hirota, N. *J. Chem. Phys.* **1991**, *95*, 6490.

$$A_{ab} = \sum_n^{\text{grid}} w_n \frac{1}{|R_s(a) - R_G(n)|} \frac{1}{|R_s(b) - R_G(n)|} \tag{7}$$

$$B_a = \sum_n^{\text{grid}} w_n \frac{1}{|r - R_G(n)|} \frac{1}{|R_s(a) - R_G(n)|} \tag{8}$$

The nuclear charge at the site a, Z_a, is trivial when all-atom expression of the sites is employed, but otherwise, it is determined via the same least-squares fitting under the conservation of total nuclear charge. The partial charge operator at each site a, $\hat{Q}_a$, is then defined by

$$\hat{Q}_a = e(-\hat{N}_a + Z_a) \tag{9}$$

so as to satisfy

$$Q_a = \langle\Psi|\hat{Q}_a|\Psi\rangle = -e\sum_{p,q}^{\text{AO}} D_{pq}\langle p|\hat{n}_a|q\rangle + Z_a e = e(-N_a + Z_a) \tag{10}$$

In the above, the partial charge at the site a, Q_a, is defined via the density matrix D_{pq}, which is considered to be a function of the set of electrostatic potentials, $\{V_b\}$. Note that only the density matrix D_{pq} is required to describe the electronic state, reflecting that $\hat{Q}_a$ is a one-electron operator.

2.1.2. CPHF Equations. We first discuss the response kernel of the RHF wave function using the CPHF equation in the following. The molecular orbitals (MO's) constructing the RHF wave function are determined by optimization of the total electronic energy E under the orthonormality condition between the occupied MO's. Therefore, the RHF procedure is to minimize the following Lagrangian W:

$$W = \tfrac{1}{2}Tr[(h + F)D] - 2Tr[\epsilon(C^\dagger SC - 1)] \tag{11}$$

where ϵ stands for the Lagrange multiplier, which is a symmetric matrix. Factor 2 is introduced to correspond ϵ with the conventional orbital energies. h, F, D, C, and S denote the one-electron integral, Fock matrix, density matrix, MO coefficients, and overlap matrix, respectively. The density matrix of the RHF wave function is written as

$$D_{pq} = \sum_i^{\text{occ}} 2C_{pi}C_{qi} \tag{12}$$

The Fock matrix is constituted by two terms: the one-electron integral and the electron-repulsion term, *i.e.*

$$F_{pq} = h_{pq} + \tfrac{1}{2}\sum_{r,s}^{\text{AO}} G_{pqrs}D_{rs} \tag{13}$$

$$G_{pqrs} = 2(pq|rs) - (pr|qs) \tag{14}$$

Under the external field or the solvated environment, the electron-field electrostatic interaction term is added to the one-electron integral h_{pq} as

$$h_{pq} = h_{0,pq} + \Delta h_{pq} \tag{15}$$

$h_{0,pq}$ means the conventional one-electron integral consisting of kinetic energy and nuclear attraction. The second term, Δh_{pq}, is expressed as

$$\Delta h_{pq} = \sum_a^{\text{site}} e\left\langle p \left| -\hat{n}_a + \frac{Z_a}{N} \right| q \right\rangle V_a \equiv \sum_a^{\text{site}} Q_{pq}^a V_a \tag{16}$$

The variational condition is given as usual:

$$W_{pi} \equiv \frac{\partial W}{\partial C_{pi}} = 0 \tag{17}$$

Consider the derivative of the orbital coefficients C_{pq}^a with respect to the external field V_a. The CPHF equation is thus derived by differentiating eq 17 as

$$\sum_q^{\text{AO}}\sum_j^{\text{MO}} W_{pi,qj}C_{qj}^a + W_{pi}^a = 0 \tag{18}$$

We introduced a brief notation in a usual way as follows:

1.

$$W_{pi,qj} \equiv \frac{\partial^2 W}{\partial C_{pi}\partial C_{qj}}$$

$$= 4\delta_{ij}(F_{pq} - S_{pq}\epsilon_{ji}) + 4\sum_{r,s}^{\text{AO}} H_{prqs}C_{sj}C_{ri} \tag{19}$$

where

$$H_{prqs} = 4(pr|qs) - (pq|rs) - (ps|qr) \tag{20}$$

2.

$$W_{pi}^a = 4\sum_q^{\text{AO}} Q_{pq}^a C_{qi} \tag{21}$$

3. The derivative C_{qj}^a is converted into MO representation to define U_{ij}^a:

$$C_{qj}^a = \sum_i^{\text{MO}} C_{qi}U_{ij}^a \tag{22}$$

where U_{ij}^a is antisymmetric,

$$U_{ij}^a + U_{ji}^a = 0 \tag{23}$$

due to the orthonormality condition of MO's.

By substituting eqs 19, 21, and 22 into eq 18, the CPHF equation is reformulated on the MO representation:

$$(\epsilon_l - \epsilon_i)U_{li}^a + \sum_j^{\text{occ}}\sum_k^{\text{vir}} H_{likj}^{(\text{MO})}U_{kj}^a = -Q_{li}^{(\text{MO}),a} \tag{24}$$

where the upper suffix (MO) indicates the MO representation and the lower suffices l, i, ... mean MO. i and j stand for the occupied MO and k and l for the virtual, respectively. Canonical MO's were employed so that ϵ has only diagonal terms expressed with one suffix, l or i. Equation 24 is the linear equation to be solved to obtain U_{li}^a. With the aid of the Hellmann−Feynman theorem,

$$\frac{\partial E}{\partial V_a} = \left\langle \Psi \left| \frac{\partial \hat{H}}{\partial V_a} \right| \Psi \right\rangle = \langle\Psi|\hat{Q}_a|\Psi\rangle = Q_a \tag{25}$$

the response kernel $(\partial Q_a/\partial V_b)_N$ is given as the second derivative of the energy as follows:

$$\frac{\partial Q_a}{\partial V_b} = \frac{\partial^2 E}{\partial V_a \partial V_b} = \langle\Psi^b|\hat{Q}_a|\Psi\rangle + \langle\Psi|\hat{Q}_a|\Psi^b\rangle$$

$$= \sum_i^{\text{occ}}\sum_j^{\text{vir}}\sum_{p,q}^{\text{AO}} 4Q_{pq}^a C_{pi}C_{qj}U_{ji}^b = \sum_i^{\text{occ}}\sum_j^{\text{vir}} 4Q_{ij}^{(\text{MO}),a}U_{ji}^b \tag{26}$$

We note that Q_{pq}^a and $Q_{ij}^{(\text{MO}),a}$ are symmetric matrices. The range of the suffix j can be restricted to the virtual space according to eq 23.

The above discussion is readily extended to the UHF case, where MO's having α-spin and β-spin have to be considered differently. The CPHF equation in the UHF case is given in the following:

$$(\epsilon_l^\alpha - \epsilon_i^\alpha)U_{li}^{\alpha,a} + 2\sum_k^{vir\alpha}\sum_j^{occ\alpha} I_{likj}^{(MO),\alpha\alpha\alpha\alpha}U_{kj}^{\alpha,a} +$$

$$2\sum_k^{vir\beta}\sum_j^{occ\beta} J_{likj}^{(MO),\alpha\alpha\beta\beta}U_{kj}^{\beta,a} = -Q_{li}^{(MO),\alpha\alpha,a} \quad (27)$$

$$(\epsilon_l^\beta - \epsilon_i^\beta)U_{li}^{\beta,a} + 2\sum_k^{vir\beta}\sum_j^{occ\beta} I_{likj}^{(MO),\beta\beta\beta\beta}U_{kj}^{\beta,a} +$$

$$2\sum_k^{vir\alpha}\sum_j^{occ\alpha} J_{likj}^{(MO),\beta\beta\alpha\alpha}U_{kj}^{\alpha,a} = -Q_{li}^{(MO),\beta\beta,a} \quad (28)$$

where

$$I_{pqrs} \equiv (pq|rs) - {}^1\!/_2\{(pr|qs) + (ps|qr)\} \quad (29)$$

$$J_{pqrs} \equiv (pq|rs) \quad (30)$$

The notations are similar with those of the RHF case except the upper suffices contain α or β to distinguish the spin states. The upper suffix (MO) denoting the MO representation is followed by the suffix α of β, which identifies the spin state of the MO of the corresponding lower suffix. The response kernel $(\partial Q_a/\partial V_b)_N$ is thus written in the UHF case using $U_{ij}^{\alpha,a}$ and $U_{ij}^{\beta,a}$ as

$$\frac{\partial Q_a}{\partial V_b} = \langle\Psi^b|\hat{Q}_a|\Psi\rangle + \langle\Psi|\hat{Q}_a|\Psi^b\rangle$$

$$= \sum_i^{occ\alpha}\sum_j^{vir\alpha}\sum_{p,q}^{AO} 2Q_{pq}^\alpha C_{pi}^\alpha C_{qj}^\alpha U_{ji}^{\alpha,b} + \sum_i^{occ\beta}\sum_j^{vir\beta}\sum_{p,q}^{AO} 2Q_{pq}^\alpha C_{pi}^\beta C_{qj}^\beta U_{ji}^{\beta,b}$$

$$= \sum_i^{occ\alpha}\sum_j^{vir\alpha} 2Q_{ij}^{(MO),\alpha\alpha,a}U_{ji}^{\alpha,b} + \sum_i^{occ\beta}\sum_j^{vir\beta} 2Q_{ij}^{(MO),\beta\beta,a}U_{ji}^{\beta,b} \quad (31)$$

2.2. Analysis of Charge Fluctuation. 2.2.1. Normal Modes. Since the response kernel $(\partial Q_a/\partial V_b)_N$ is a symmetric matrix (see eq 26), it can be diagonalized via a unitary transformation that identifies the normal modes:

$$P^\dagger KP = \Lambda \quad (32)$$

where K denotes the response kernel, $K_{ab} = K_{ba} = \partial Q_a/\partial V_b$. $P = (p_1, p_2, ..., p_{N_{site}})$ is the unitary transformation matrix, and p_i stands for the ith normal mode vector. Λ is the diagonal matrix:

$$\Lambda_{ab} = \lambda_a\delta_{ab} \quad (\lambda_1 \le \lambda_2 \le ... \le \lambda_{N_{site}}) \quad (33)$$

The normal modes defined above provide a useful means to analyze the charge fluctuation for the following reasons. First, the actual charge fluctuation in solution can be well described only with a few softest modes; the other harder modes contribute little and have less significance. The softest mode means p_1, the mode having the most negative eigenvalue λ_1 of the response kernel. Note that all of the eigenvalues except $\lambda_{N_{site}}$ are negative due to the stability of the system, since positive electrostatic potential induces negative charge and vice versa. One eigenvalue $\lambda_{N_{site}}$ is invariably zero, corresponding to the uniform potential ($p_{1N_{site}} = p_{2N_{site}} = ... = p_{N_{site}N_{site}}$). The softest mode is most important to characterize the charge fluctuation; the difference between a parent molecule and the radical largely comes from it, as will be discussed later. Second, the normal mode analysis is suitable especially to the π-electron systems where the charge polarization is essentially delocalized. The normal modes are of great help to understand the correlated polarization on the different sites. If the molecule has a symmetry, we can make use of it to simplify the analysis, because each normal mode as well as a canonical orbital belongs to a certain irreducible representation. The MO distortion contingent to a normal mode is usually well expressed with a few molecular orbitals.

2.2.2. Intrinsic Soft MO Pairs. The solution of the CPHF equation (*i.e.* U_{ij}^a of eq 24 or $U_{ij}^{\alpha,a}$ and $U_{ij}^{\beta,a}$ of eqs 27 and 28) is the derivative of the MO coefficients with respect to V_a, the electrostatic potential at the site a. The contribution of the softest normal mode p_1 to the MO derivatives is accordingly given as

$$U_{ij} = \sum_a^{site} p_{a1}U_{ij}^a \quad (34)$$

for the RHF case. In the left-hand side of eq 34, the superscript a over the derivative matrix U is omitted, which designates the derivative of the softest mode. Note that the subscript i of U_{ij} stands for a virtual MO and j for a occupied one. We introduce a new set of the occupied and virtual orbitals $\{\phi_i\}$ derived from the original MO set $\{\psi_i\}$:

$$\phi_i^{occ} = \sum_j^{occ} V_{ij}^{occ}\psi_j^{occ}, \quad \phi_i^{vir} = \sum_j^{vir} V_{ij}^{vir}\psi_j^{vir} \quad (35)$$

so that the new representation of U is diagonal:

$$[(V^{vir})^\dagger UV^{occ}]_{ij} = u_i\delta_{ij} \quad (u_1{}^2 \ge u_2{}^2 \ge ...) \quad (36)$$

The unitary matrices V^{vir} and V^{occ} are calculated in the analogue of the standard eigenvalue problem.[32] V^{vir} is obtained by diagonalizing the square matrix $UU^\dagger$:

$$[(V^{vir})^\dagger\cdot(UU^\dagger)\cdot V^{vir}]_{ij} = u_i{}^2\delta_{ij} \quad (37)$$

and V^{occ} by $U^\dagger U$:

$$[(V^{occ})^\dagger\cdot(U^\dagger U)\cdot V^{occ}]_{ij} = u_i{}^2\delta_{ij} \quad (38)$$

Equations 37 and 38 are for the RHF case. The UHF case can be treated in the same way with distinct spin suffices.

The new representation derives pairs of occupied and virtual MO; the virtual MO of each pair suffices to express the distortion of the corresponding occupied MO. The ith new occupied MO ϕ_i^{occ} is modified under the small perturbation ($p_{a1}\delta V$ at each site a) into

$$\phi_i^{occ} \rightarrow \phi_i^{occ} + u_i\phi_i^{vir}\delta V \quad (39)$$

The squared eigenvalue $u_i{}^2$ indicates the extent of the distortion of ith MO. Since the sum of the squared eigenvalues $\sum_i u_i{}^2 = \sum_i^{occ}\sum_j^{vir} U_{ij}{}^2$, which is invariant under any unitary transformation, evaluates the total distortion, the MO pairs introduced above provide a proper decomposition of the total distortion into each MO pair. Among the MO pairs, some pairs having large squared eigenvalues ($u_1{}^2$, $u_2{}^2$, *etc.*) are particularly important to represent the electronic distortion. We call them the "soft MO pairs" for the softest normal mode. Although we focus on the softest mode at present, this concept can be readily generalized to other perturbations that give rise to the distortion of MO's.

The eigenvalue of the charge polarization for the softest mode, λ_1 in eq 33, is also decomposable using the MO pairs;

$$\lambda_1 = \sum_{a,b} p_{a1}p_{b1}\frac{\partial Q_a}{\partial V_b} = 2p_{a1}p_{b1}\langle\Psi|\hat{Q}_a|\Psi^b\rangle$$

$$= \sum_{a,b} 2p_{a1}p_{b1}\sum_i^{occ}\sum_j^{vir} 2\left\langle\psi_i^{occ}\left|e\left(-\hat{n}_a + \frac{Z_a}{N}\right)\right|\psi_j^{vir}\right\rangle U_{ji}^b$$

$$= \sum_a 4p_{a1}\sum_i^{occ}\left\langle\phi_i^{occ}\left|e\left(-\hat{n}_a + \frac{Z_a}{N}\right)\right|\phi_i^{vir}\right\rangle u_i$$

(32) Amos, A. T.; Hall, G. G. *Proc. R. Soc. London* **1961**, *A263*, 483.

Intramolecular Charge Polarization

J. Am. Chem. Soc., Vol. 119, No. 17, 1997 4025

$$= \sum_i 4u_i \langle \phi_i^{occ}| - \sum_a ep_{a1}\hat{n}_a|\phi_i^{vir}\rangle$$

$$\equiv \sum_i^{occ} 4u_i T_i \quad \text{for} \quad \text{RHF} \tag{40}$$

$$\lambda_1 = \sum_i^{occ\alpha} 2u_i^{\alpha} T_i^{\alpha} + \sum_i^{occ\beta} 2u_i^{\beta} T_i^{\beta} \quad \text{for} \quad \text{UHF} \tag{41}$$

Equations 40 and 41 indicate that the charge polarization is composed of two factors: the MO distortion u_i and the transition moment T_i. The intrinsic soft MO pairs for the UHF case are obtained by a procedure similar to that above. In this case, the transformations of MO's are performed for the α- and β-spin orbitals. The resultant charge polarization of the softest mode is expressed by eq 41.

2.2.3. Decomposition Based on Localized Orbitals. Although the intrinsic soft MO pairs introduced in section 2.2.2 have the distinguished features as described above, other representations of MO's are sometimes utilized to express the MO distortion. For example, localized orbitals, which provide a clear picture of the chemical bonds, can be more suitable for qualitative discussion of the MO distortion than the intrinsic soft MO's, in case that the latter orbitals are hard to be simply assigned. Therefore, we propose here another decomposition procedure based on the localized orbitals. We define a set of localized orbitals $\{\phi_i^L\}$ via a unitary transformation of the occupied orbitals of the intrinsic soft MO pairs $\{\phi_j^{occ}\}$:

$$\phi_i^L = \sum_j^{occ} \phi_j^{occ} O_{ji} \tag{42}$$

We employed the Boys' localization procedure[33,34] to define O_{ji}, though another method of localization is also available. The eigenvalue of the softest normal mode λ_1 is expressed using the localized orbitals as follows (*cf.* eq 40):

$$\lambda_1 = \sum_i^{occ} 4u_i T_i = \sum_j^{occ} (\sum_i^{occ} 4O_{ij} u_i T_i O_{ij}) \tag{43}$$

for the RHF case, where the suffix j denotes the localized orbitals. The original decomposition with the intrinsic soft MO pairs has only one suffix i because it retains the diagonal expression of the deformability matrix u_i and the transition matrix T_i between the occupied and virtual MO space. The decomposition based on the localized orbitals breaks the diagonality so that it becomes impossible to define the unique counterpart virtual orbital for each localized occupied orbital. This is a weak point of this procedure using the localized orbitals compared to the original one, while this decomposition scheme is amenable to the qualitative assignment and interpretation of the MO's. The decomposition scheme based on the localized orbitals is particularly useful to the nonaromatic systems where the local bond orbitals play a predominant role rather than the delocalized π-electrons. We applied this scheme to acetone, 2-hydroxypropyl radical, and β-propyl radical to analyze the MO distortion.

2.2.4. σ and π Decomposition. When we discuss the MO distortion of aromatic systems, the contributions of the σ- and π-electrons can be discriminated. We decompose λ_1, the eigenvalue of the softest normal mode, into these contributions. Equation 40 derives the AO-based expression of λ_1 as

$$\lambda_1 = \sum_i 4u_i T_i$$

$$= \sum_i 4u_i \langle \phi_i^{occ}| - \sum_a ep_{a1}\hat{n}_a|\phi_i^{vir}\rangle$$

$$= \sum_{p,q}^{AO} (\sum_i P_{pq,i}) Q_{pq} \quad \text{for} \quad \text{RHF} \tag{44}$$

where

$$Q_{pq} = \langle p| \sum_a ep_{a1}\hat{n}_a|q\rangle \tag{45}$$

$$P_{pq,i} = 4u_i C_{pi} C_{qi} \tag{46}$$

The atomic orbitals are classified either σ or π in a planar molecule. Therefore, the double summation over p and q in eq 44 is decomposed into the following four terms: σ(occ)−σ(vir), σ(occ)−π(vir), π(occ)−σ(vir), and π(occ)−π(vir). This classification is not rigorous for a nonplanar molecule, but it still can be applied to the pyrazinyl radical to characterize the MO distortion, since all the constituting atoms except H_{11} ($N_1 \sim H_{10}$) retain an approximate plane (see Figure 1). The σ and π characters are mixed in the nonplanar radical, while they are definitely separated in the planar parent molecule.

3. Results and Discussion

The *ab initio* MO calculations, closed-shell RHF or UHF, were carried out with the HONDO package.[35] The calculation of the response kernel based on the CPHF equation, and further analyses were made using our original code incorporated into the HONDO package. The basis set employed in the present calculations was mainly the Huzinaga−Dunning−Raffenetti (9s5p1d/4s1p)/[3s2p1d/2s1p] basis,[36,37] which has double-ζ plus polarization (DZP) quality. To check the accuracy of the basis set, tentative calculation was also performed using the DZP basis set augmented with some diffuse anion bases[36] that facilitate the charge polarization. The SCF MO calculations had to be done with a tighter criterion of convergence than usual, since the quality of the wave function is rather significant for the following analysis. The convergence criterion was set to be 1.0×10^{-9} for the maximum difference of the density matrix elements to those of the preceding iteration.

The molecular geometries employed in the present work are either experimental or *ab initio* optimized. The geometry of benzene is experimentally determined: $R_{C-C} = 1.399$ Å and $R_{C-H} = 1.101$ Å with D_{6h} symmetry.[38] The other species were all optimized through the *ab initio* calculations because the geometries of the radicals have been experimentally unknown. The optimized geometries are displayed in Figure 1. Experimental data are available for pyrazine and acetone,[38] but the discrepancy is insignificant (within 0.02 Å or 0.6°).

We chose all the atomic positions including hydrogen as the intramolecular sites, except when we explicitly mentioned the extended-site model. The grid points to evaluate the electrostatic potential around the molecule were placed on the molecular envelope that consists of united spheres around all atoms of the molecule. The weight factor w_n of eq 4 was set to be unity. The radii of the atomic spheres were standard van der Waals (vdW) radii[39] added with the margin of 2.5 bohr. The geometry of the grid points accommodated itself to the molecular symmetry so as to preserve the symmetry of charge distribution. The number of points was 3946 for pyrazine.

(33) Foster, J. M.; Boys, S. F. *Rev. Mod. Phys.* **1960**, *32*, 300.
(34) Weinstein, H.; Pauncz, R.; Cohen, M. *Adv. At. Mol. Phys.* **1971**, *7*, 97.

(35) Dupuis, M.; Watts, J. D.; Villar, H. O.; Hurst, G. J. B. HONDO Ver. 7.0. *QCPE* **1987**, *544*.
(36) Dunning, T. H., Jr.; Hay, P. J. In *Methods of Electronic Structure Theory*, III; H. F. S., Ed.; Plenum: New York, 1977; Vol. 3 of *Modern Theoretical Chemistry*, Chapter 1.
(37) This basis set has been prepared in the HONDO package with the name of "DZP".
(38) Lide, D. R., Ed. *Handbook of Chemistry and Physics*, 73rd ed.; CRC: Boca Raton, FL, 1992.
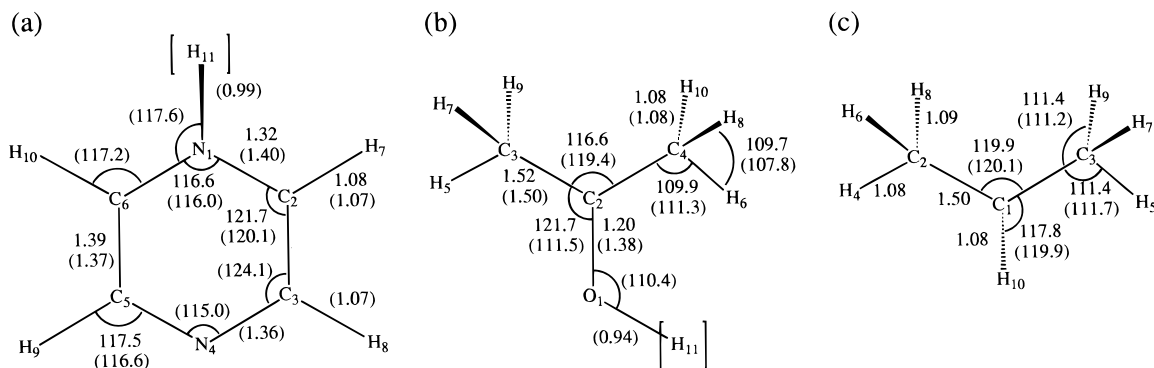(39) Bondi, A. *J. Phys. Chem.* **1964**, *68*, 441.

Figure 1. Molecular geometries of (a) pyrazine and pyrazinyl radical, (b) acetone and 2-hydroxypropyl radical, and (c) β-propyl radical. These geometries were *ab initio* optimized (see the text). These figures also indicate atomic serial numbers of each molecule defined in convenience. Units: Å for distances and degrees for angles. Values in parentheses mean those of the radicals. (a) Pyrazine is planar with D_{2h}. Pyrazinyl radical has a mirror symmetry of the plane intersecting N_1–N_4 axis. The out-of-plane angle of 11-(1,2,6) is 28.8°. The calculated energy is −262.730 060 hartrees for pyrazine and −263.288 479 hartrees for pyrazinyl radical using the DZP basis set. (b) Acetone has C_{2v} symmetry. Dihedral and out-of-plane angles of 2-hydroxypropyl radical are as follows: out-of-plane 1-(2,3,4), 37.3°; dihedral 11-1-2-3, 179.4°; 11-1-2-4, 38.5°; 5-3-2-1, 47.1°; 6-4-2-1, 50.2°; 7-3-2-1, 167.7°; 8-4-2-1, 69.9°; 9-3-2-1, 72.4°; 10-4-2-1, 170.1°. The calculated energy is −192.008 490 hartrees for acetone and −192.547 611 hartrees for 2-hydroxypropyl radical using the DZP basis set. (c) The two geometries of β-propyl radical are displayed: the equilibrium one with C_s symmetry (values without parentheses) and the "planar" geometry with C_{2v}. The values in parentheses are those of the planar geometry that are different to those of the equilibrium geometry. The out-of-plane angle of 10-(1,2,3) is 21.1° for the equilibrium and 0° for planar.

3.1. Benzene. We chose benzene as a prototype of the analysis for the following reasons. First, it is a typical example of an aromatic π-electron system, providing a reference for other aromatic systems like pyrazine or benzophenone. Second, it is highly symmetric as to exemplify the D_{6h} point group. The high symmetry poses a hard selection rule on the orbital mixing, which greatly simplifies the subsequent analysis. For example, we need not take account of the $\sigma-\pi$ mixing owing to the planar symmetry.

The calculated RHF energy of benzene was −230.740 796 hartrees. The partial charges on the carbon site and hydrogen site were −0.151 and 0.151, respectively. Figure 2 demonstrates the normal modes and their eigenvalues λ_i of the response kernel (see eq 32). These eigenvalues corroborate the former discussion that all are negative except for one, $\lambda_{N_{\text{site}}} = \lambda_{12} = 0$, which corresponds to the uniform potential. All modes are labeled with the irreducible representations of D_{6h} also displayed in Figure 2. The figure shows that the 1−6 and 7−12 modes repeat the same pattern of symmetry, but with significant difference. The former group has large amplitudes chiefly on the carbon atoms, while the latter, on the hydrogen atoms; the charge polarization on the carbon skeleton is pronounced on the relatively soft 1−6 modes. When we observe the nodal patterns of the 1−6 modes besides their symmetry, we find that they are quite analogous with those of the valence π MO's. It is commonly known that among the valence π orbitals the more nodes an orbital has, the higher its orbital energy is. The same order is also seen in the softness of the charge polarization modes, indicating that a mode with more nodes is softer. This fact originates from a rule that adjacent sites tend to induce opposite charge. This rule is expressed as

$$\text{(i)}\quad \partial Q_a/\partial V_b < 0$$

$$\text{(ii)}\quad \partial Q_a/\partial V_b > 0,\quad \text{if sites } a \text{ and } b \text{ are adjacent}$$

which generally holds to any other molecules treated here including π and σ systems.

The soft 1−5 modes are characterized qualitatively via the distortion of the valence π orbitals. This is evident when we observe the derivative matrix of each mode. The derivative matrix of the MO coefficients for the kth normal mode, U_{ij}^k, is given as
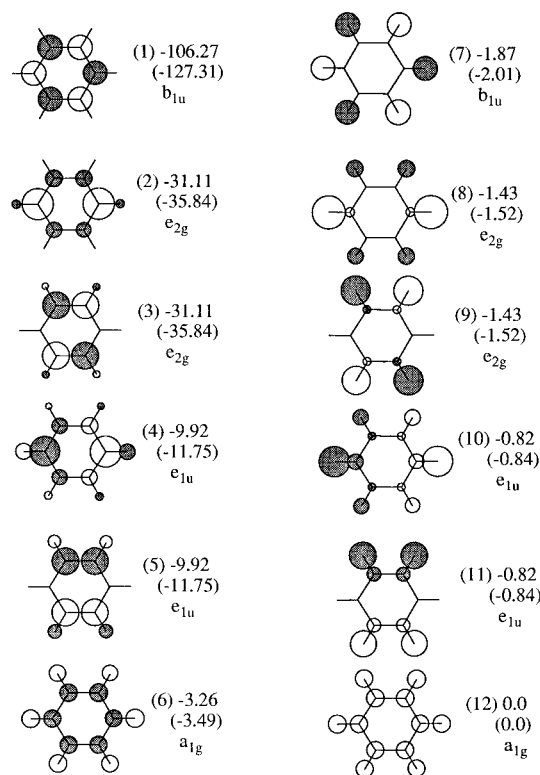
Figure 2. Normal modes and their eigenvalues of the response kernel of benzene. The radius of the circle at each site is proportional to the amplitude on the site of the eigenvector. The color of the circle (white or black) indicates sign of the amplitude. Values in parentheses are the eigenvalues obtained with the augmented basis set (see the text). Basis set dependence of the normal modes is negligible in this figure.

$$U_{ij}^k = \sum_a^{\text{site}} p_{ak} U_{ij}^a \qquad (47)$$

The principal components of U_{ij}^k ($k = 1 \sim 5$) are displayed in Table 1. As we see that all of these terms represent valence $\pi-\pi$ mixing, the valence π orbitals play the dominant role for the orbital distortion. The qualitative pattern of the orbital mixing among the π orbitals is readily understandable from the selection rule imposed by the symmetry.

Table 1. Principal Components of the MO Derivative Matrix U_{ij}^k for the kth Mode of Benzene[a]

mode k	occ j	vir i	U_{ij}^k	occ j	vir i	U_{ij}^k	occ j	vir i	U_{ij}^k
1	20	1	−5.64	21	2	−5.64	17	8	−2.53
2	17	2	−1.39	21	8	−0.85			
3	17	1	−1.39	20	8	−0.85			
4	21	1	0.98	20	2	0.98			
5	20	1	−0.98	21	2	0.98			

MO	symmetry	ϵ/hartree	MO	symmetry	ϵ/hartree
17th occupied	a_{2u}	−0.498 90	1st virtual	e_{2u}	0.124 81
20	e_{1g}	−0.335 55	2	e_{2u}	0.124 81
21	e_{1g}	−0.335 55	8	b_{2g}	0.324 97

[a] All of the six orbitals, *i.e.* 17th, 20th, and 21th occupied and 1st, 2nd, and 8th virtual, are valence π orbitals. The symmetries and orbital energies ϵ are shown in the lower portion of the table.

Table 2. Decomposition of the Softest Normal Mode of Benzene using the Intrinsic MO Pairs. (Nine Principal Pairs Are Displayed)

i	u_i^2	u_i	T_i	$4u_iT_i$	symmetry: occ-vir	
1	32.917	−5.737	1.299	−29.810	e_{1g}−e_{2u}	(π−π)
2	32.917	−5.737	1.299	−29.810	e_{1g}−e_{2u}	(π−π)
3	6.887	−2.624	1.435	−15.065	a_{2u}−b_{2g}	(π−π)
4	1.871	−1.368	1.222	−6.687	e_{1u}−e_{2g}	(σ−σ)
5	1.871	−1.368	1.222	−6.687	e_{1u}−e_{2g}	(σ−σ)
6	1.745	−1.321	1.033	−5.460	e_{2g}−e_{1u}	(σ−σ)
7	1.745	−1.321	1.033	−5.460	e_{2g}−e_{1u}	(σ−σ)
8	1.306	−1.143	1.145	−5.234	a_{1g}−b_{1u}	(σ−σ)
9	1.199	−1.095	0.793	−3.473	b_{1u}−a_{1g}	(σ−σ)
total	83.142			−106.267		

Table 3. Polarizability of Benzene, Pyrazine (py), Pyrazinyl Radical (pyH), Acetone (ac), and 2-Hydroxypropyl Radical (acH)[a]

	principal components			isotropic
benzene	10.83 (11.31)	10.83 (11.31)	4.03 (5.56)	8.56 (9.39)
py	9.59 (10.01)	8.01 (8.60)	3.47 (4.51)	7.02 (7.71)
pyH	8.81 (9.68)	8.32 (9.13)	3.63 (3.78)	6.92 (7.53)
ac	5.70 (6.12)	5.07 (5.29)	4.09 (4.31)	4.96 (5.24)
acH	5.65 (5.90)	5.29 (5.67)	4.40 (4.82)	5.11 (5.46)

[a] Values in parentheses were calculated using the DZP basis augmented with the anion bases on N and C atoms.[36] Units: Å^3.

We further analyze the softest normal mode using the intrinsic MO pairs introduced in section 2; the result of the decomposition is given in Table 2. The 1−3 MO pairs represent the π−π mixing, which constitute about 75% of the total polarization λ_1 = −106.267. These soft MO's are almost identical to the canonical MO's; the coefficients of the original MO's exceed 0.97 in the corresponding new MO's. This invariance partly comes from the high symmetry of benzene that largely restricts the orbital mixing.

Finally, we checked the accuracy of the DZP basis set by comparing it with the DZP basis set augmented with the diffuse anion bases. A diffuse p-type basis with the exponent of 0.034, which is originally devised to express anion states,[36] is put on each carbon atom to facilitate the charge polarization. The total energy was −230.741 539 hartrees with the augmented basis set, which shows 7.4×10^{-4} hartree stabilization from the DZP basis alone. Figure 2 also displays the eigenvalues obtained with the augmented basis set. The result of the augmented basis set gives about 20% larger value at maximum. The deviation is of a similar trend with that of the polarizability as seen in Table 3, where the value of the augmented basis set is about 10% enhanced. The DZP basis set is not sufficient to calculate the absolute value of the response kernel as well as the polarizability for quantitative purpose, but we can utilize it to discuss the relative enhancement of the charge sensitivity.

3.2. Pyrazine and Pyrazinyl Radical. We discuss here the charge polarization of pyrazine and pyrazinyl radical. The

Table 4. Partial Charges at the Sites of Pyrazine (py) and Pyrazinyl Radical (pyH) and Acetone (ac) and 2-Hydroxypropyl Radical (acH)[a]

site		py	pyH
1	N	−0.454	−0.296
2	C	0.150	−0.305
3	C	0.150	0.353
4	N	−0.454	−0.591
5	C	0.150	0.353
6	C	0.150	−0.305
7	H	0.077	0.172
8	H	0.077	0.038
9	H	0.077	0.038
10	H	0.077	0.172
11	H		0.371

dipole moment/D		
partial charge	0.000	3.504
ab initio	0.000	3.497

site		ac	acH
1	O	−0.595	−0.586
2	C	0.836	0.287
3	C	−0.554	−0.587
4	C	−0.554	−0.554
5	H	0.153	0.175
6	H	0.153	0.137
7	H	0.140	0.160
8	H	0.140	0.180
9	H	0.140	0.199
10	H	0.140	0.164
11	H		0.426

dipole moment/D		
partial charge	3.239	1.594
ab initio	3.231	1.601

[a] The site number of each site is displayed in Figure 1. The resultant dipole moments and the *ab initio* values are also compared.

partial charges on the atomic sites are given in Table 4 along with the dipole moments calculated with the classical model based on the partial charges. The partial charges well reproduced the dipole moments calculated by the *ab initio* method. As seen in Table 5, the response kernel $(\partial Q_a/\partial V_b)_N$ of the two species demonstrates a surprising difference; the radical is much more polarizable than the parent. We mention that this difference does not mean that pyrazinyl radical has a much larger polarizability than pyrazine. Table 3 shows that the usual polarizabilities of the two species are close within the same basis set. The particular softness of the radical does not manifest itself by uniform electric field, but it does by local fluctuated field. The normal mode analysis in Figure 3 reveals that the striking softness of the radical is mainly originated from the first (softest) mode although the other modes, especially a″

Table 5.   Response Kernel $(\partial Q_n/\partial V_b)_N$ of (a) Pyrazine and (b) Pyrazinyl Radical[a]

(a) Pyrazine

	1	2	3	4	5	6	7	8	9	10
1	−11.622	4.440	−7.169	−7.169	11.329	11.329	1.059	1.059	−1.629	−1.629
2	4.440	−11.622	11.329	11.329	−7.169	−7.169	−1.629	−1.629	1.059	1.059
3	−7.169	11.329	−24.538	−6.527	16.907	7.617	5.894	0.370	−2.760	−1.124
4	−7.169	11.329	−6.527	−24.538	7.617	16.907	0.370	5.894	−1.124	−2.760
5	11.329	−7.619	16.907	7.617	−24.538	−6.527	−2.760	−1.124	5.894	0.370
6	11.329	−7.169	7.617	16.907	−6.527	−24.538	−1.124	−2.760	0.370	5.894
7	1.059	−1.629	5.894	0.370	−2.760	−1.124	−2.825	0.176	0.560	0.277
8	1.059	−1.629	0.370	5.894	−1.124	−2.760	0.176	−2.825	0.277	0.560
9	−1.629	1.059	−2.760	−1.124	5.894	0.370	0.560	0.277	−2.825	0.176
10	−1.629	1.059	−1.124	−2.760	0.370	5.894	0.277	0.560	0.176	−2.825

(b) Pyrazinyl Radical

	1	2	3	4	5	6	7	8	9	10	11
1	−106.358	79.257	−41.249	24.768	−41.249	79.257	−16.848	4.402	4.402	−16.848	30.467
2	79.257	−74.105	42.404	−21.827	32.147	−56.266	17.074	−5.305	−3.622	11.527	−21.284
3	−41.249	42.404	−36.914	18.119	−19.004	32.147	−8.465	7.229	1.747	−6.786	10.771
4	24.768	−21.827	18.119	−15.045	18.119	−21.827	4.461	−2.355	−2.355	4.461	−6.518
5	−41.249	32.147	−19.004	18.119	−36.914	42.404	−6.786	1.747	7.229	−8.465	10.771
6	79.257	−56.266	32.147	−21.827	42.404	−74.105	11.527	−3.622	−5.305	17.074	−21.284
7	−16.848	17.074	−8.465	4.461	−6.786	11.527	−5.340	1.108	0.850	−2.252	4.672
8	4.402	−5.305	7.229	−2.355	1.747	−3.622	1.108	−3.022	0.016	0.850	−1.048
9	4.402	−3.622	1.747	−2.355	7.229	−5.305	0.850	0.016	−3.022	1.108	−1.048
10	−16.848	11.527	−6.786	4.461	−8.465	17.074	−2.252	0.850	1.108	−5.340	4.672
11	30.467	−21.284	10.771	−6.518	10.771	−21.284	4.672	−1.048	−1.048	4.672	−10.171

[a] RHF and UHF wave functions were employed, respectively, both with the DZP basis set. Units: au.

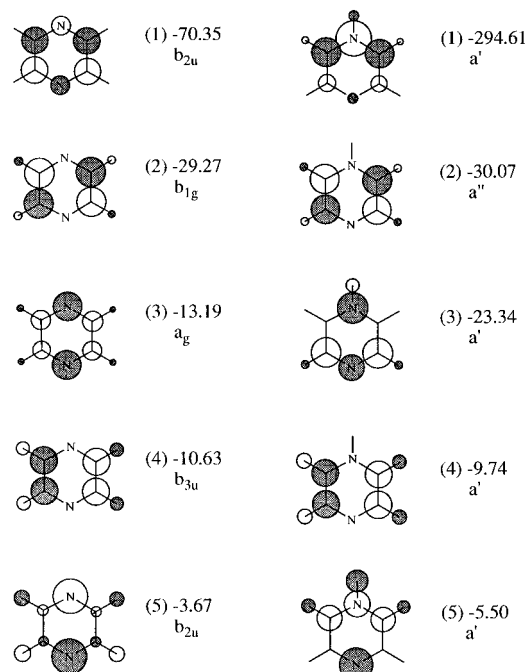(a) pyrazine   (b) pyrazinyl radical

Figure 3. Normal modes and their eigenvalues of the response kernel of (a) pyrazine and (b) pyrazinyl radical. See Figure 2.

modes, are little altered. The eigenvalue λ_1 of the radical, −294.61, is about 4 times larger than that of the parent, −70.35, though the nodal patterns are qualitatively similar, both indicating alternating an amplitude pattern among the ring skeleton. To elucidate the difference of the softest mode, we further analyze it with the help of the soft MO pairs introduced in section 2.

3.2.1. Pyrazine. The softest mode of pyrazine was decomposed using the intrinsic soft MO pairs in Table 6a. The total MO distortion of pyrazine ($\sum_i u_i^2 = 39.8$) is substantially reduced from that of benzene ($\sum_i u_i^2 = 83.1$). Among the five principal soft MO pairs, 1, 2, and 5 indicate $\pi-\pi$ mixing while

Table 6.   Decomposition of the Softest Normal Mode of (a) Pyrazine and (b) Pyrazinyl Radical using the Intrinsic MO Pairs (Nine Principal Pairs are Displayed)

(a) Pyrazine

i	u_i^2	u_i	T_i	$4u_iT_i$	symmetry: occ-vir	
1	21.065	−4.590	1.306	−23.972	b_{2g}−a_u	$(\pi-\pi)$
2	5.440	−2.332	0.613	−5.715	b_{3g}−b_{1u}	$(\pi-\pi)$
3	3.906	−1.976	1.585	−12.530	b_{2u}−a_g	$(\sigma-\sigma)$
4	3.607	−1.899	1.560	−11.848	a_g−b_{2u}	$(\sigma-\sigma)$
5	3.356	−1.832	1.071	−7.852	b_{1u}−b_{3g}	$(\pi-\pi)$
6	0.719	−0.848	0.746	−2.529	b_{3u}−b_{1g}	$(\sigma-\sigma)$
7	0.550	−0.742	0.537	−1.595	b_{1g}−b_{3u}	$(\sigma-\sigma)$
8	0.369	−0.608	0.578	−1.406	a_g−b_{2u}	$(\sigma-\sigma)$
9	0.337	−0.580	0.469	−1.088	b_{2u}−a_g	$(\sigma-\sigma)$
total	39.826			−70.350		

(b) Pyrazinyl Radical. (1) α Spin

i	$(u_i^\alpha)^2$	u_i^α	T_i^α	$2u_i^\alpha T_i^\alpha$	occ. MO
1	24.733	−4.973	3.911	−38.905	unpaired MO
2	21.023	−4.585	3.751	−34.397	α'' valence π
3	11.212	−3.348	3.190	−21.362	lone pair at N_1
4	4.801	−2.191	2.178	−9.545	localized at N_4
5	2.796	−1.672	1.964	−6.567	localized at N_4
6	2.656	−1.630	2.083	−6.790	
7	2.376	−1.541	2.638	−8.133	
8	2.069	−1.439	1.846	−5.311	
9	1.612	−1.270	1.667	−4.233	
total	75.419			−144.093	

(2) β Spin

i	$(u_i^\beta)^2$	u_i^β	T_i^β	$2u_i^\beta T_i^\beta$	occ. MO
1	37.732	−6.143	3.558	−43.714	lone pair at N_1
2	25.518	−5.052	3.302	−33.364	α'' valence π
3	13.449	−3.667	2.555	−18.740	localized at N_4
4	9.088	−3.015	2.612	−15.750	localized at N_4
5	4.076	−2.019	2.422	−9.782	
6	3.014	−1.736	2.323	−8.067	
7	2.831	−1.683	2.759	−9.284	
8	0.712	−0.844	2.111	−3.563	
9	0.702	−0.838	1.319	−2.211	
total	98.513			−150.515	

3 and 4 indicate $\sigma-\sigma$. The three $\pi-\pi$ pairs apparently retain the character of the valence π MO pairs of benzene. The first

and second MO pairs correspond to the softest degenerate pairs of benzene, and the fifth pair to the third pair of benzene. The softest degenerate pairs of benzene are splitted in pyrazine so that the $b_{2g}-a_u$ MO pair (no amplitudes on the N atoms) becomes softer than the other $b_{3g}-b_{1u}$ pair. A distinct difference from benzene, however, is that the contribution of the valence π orbitals is not so predominant in pyrazine. Table 6 shows that the third or fourth MO pair ($\sigma-\sigma$) makes even larger contribution to the eigenvalue λ_1 than the second pair ($\pi-\pi$) owing to the large transition moment T_i. We found that the large transition moments of the σ pairs largely come from the antibonding character of the virtual counterparts. The role of σ^* orbitals will be extensively discussed in the following section.

3.2.2. Pyrazinyl Radical. As shown in Figure 3, the first normal mode of pyrazinyl radical is particularly sensitive to the field perturbation compared with that of pyrazine. To understand the remarkable sensitivity of the softest mode, the decomposition analysis using the soft MO pairs was carried out, and the result is displayed in Table 6b. Before comparing the radical to the parent, we briefly describe some features of the soft MO pairs of the radical. The characters of the principal occupied MO's are listed also in Table 6b.

The occupied orbital of the first α MO pair is nearly identical to the unpaired orbital of the radical. To summarize the assignment, the MO distortion of pyrazinyl radical for the softest mode is mainly attributed to the deformation of the unpaired π orbital, the lone pair orbital at the N_1 site, and the a'' valence π orbital. Note that the hydrogen H_{11} is not planarly connected to N_1 (*cf.* Figure 1) so that the π orbital at the N_1 site takes on the character of lone pair. The virtual counterpart orbitals of the above pairs are generally complicated due to the σ^* character. Mixing of σ and π character is much more thorough in the virtual orbitals than in occupied so that simple assignment of the virtual orbitals is impossible.

We further make quantitative comments on these soft MO pairs. When we compare the α and β pairs equivalent in character in Table 6b, the difference between the third α pair and the first β pair is conspicuous, $2u_3^{\alpha}T_3^{\alpha} = -18.74$ and $2u_1^{\beta}T_1^{\beta} = -38.91$, though the occupied MO's of these MO pairs are quite similar. The difference comes from the u_i values in Table 6b, $|u_3^{\alpha}| = 3.35$ and $|u_1^{\beta}| = 6.14$, although the transition moments T_i does not so differ, $|T_3^{\alpha}| = 3.19$ and $|T_1^{\beta}| = 3.56$. This implies that the localized α orbital at N_1 is less deformable than the β orbital. The difference is obviously derived from the existence of the unpaired α electron. The unpaired α orbital, which has a' symmetry, affects the exchange interaction to the α orbital to stabilize it selectively. The same tendency is also observed in the localized orbitals at the N_4 site. It is also noteworthy that the contribution of the first α pair, or the unpaired radical orbital, is not dominant to λ_1, the eigenvalue of the softest mode, of the radical. The first β pair makes even larger contribution than the first α pair.

When we explain the remarkable enhancement of λ_1 of pyrazinyl radical, we first note that it is by no means solely attributed to the unpaired radical orbital, since the contribution of the first α MO pair ($2u_1^{\alpha}T_1^{\alpha} = -38.91$) is far short of the enhancement. Table 6 shows that the contribution of the soft pairs of the radical is generally augmented, and the difference largely comes from the transition moment T_i rather than the deformability u_i. The increase of the transition moment suggests significant modification of the relevant orbitals, especially the virtual orbitals, of these pairs. We mentioned previously that the virtual orbitals of these pairs are particularly modified owing to the inclusion of the σ^* character. Therefore, we performed the σ and π decomposition described in section 2.2.4, and the

Table 7. σ and π Components of λ_1 of Pyrazinyl Radical (occ−vir) (See Eq 44)

(1) α Spin

MO pair	$\sigma-\sigma$	$\sigma-\pi$	$\pi-\sigma$	$\pi-\pi$	total
1	−0.109	−1.943	−31.738	−5.115	−38.905
2	−0.524	−3.536	−25.754	−4.583	−34.397
3	−2.036	−0.674	−18.246	−0.407	−21.362
4	−1.926	−1.382	−5.195	−1.042	−9.545
5	−1.207	−4.854	−0.842	0.337	−6.567

(2) β Spin

MO pair	$\sigma-\sigma$	$\sigma-\pi$	$\pi-\sigma$	$\pi-\pi$	total
1	−1.635	−7.707	−29.834	−4.539	−43.714
2	−0.729	−8.679	−17.666	−6.290	−33.364
3	−2.383	−4.194	−10.387	−1.777	−18.740
4	−2.696	−4.555	−7.638	−0.861	−15.750

(3) Total

	$\sigma-\sigma$	$\sigma-\pi$	$\pi-\sigma$	$\pi-\pi$	total
total	−25.648	−86.517	−159.543	−22.901	−294.608

four components of pyrazinyl radical, *i.e.* σ(occ)−σ(vir), σ(occ)−π(vir), π(occ)−σ(vir), and π(occ)−π(vir), are displayed in Table 7. The result clearly shows that the π(occ)−σ(vir) term is quite significant and even dominant in the principal soft MO pairs. This means that the inclusion of σ character into the virtual orbitals is the main source of the enhancement of λ_1.

We examined the above conclusion using an extended-site model of pyrazine and its radical which has some extra sites out of the molecular plane, and thus corroborated that inclusion of the nonplanar sites does not affect the present conclusion. We employed the tentative model in order to explicitly investigate the nonplanar perturbation of the external field because the all-atom model of a (nearly) planar molecule does not fully take account of the nonplanar perturbation. In the extended-site model, the nonplanar virtual sites were put 1.74 bohr above and below the nitrogen atoms and 2.09 bohr the carbon atoms, where the diffuse components of the DZP $2p_z$ basis functions ($\alpha = 0.1654$ for nitrogen, $\alpha = 0.1146$ for carbon) have the maximum amplitudes. In the pyrazinyl radical with the nonplanar extra hydrogen H_{11}, another extra site was put as nearly the mirror image of H_{11} to remove possible artificial nonplanar effect due to the nonplanar site configuration. The numbers of the total sites became 22 for pyrazine and 24 for pyrazinyl radical. The obtained eigenvalues of the softest normal mode λ_1 were −115.31 for pyrazine and −292.72 for pyrazinyl radical, respectively, which again shows the significant enhancement. We also found that the softest normal mode has little components of the virtual sites and that the (nearly) out-of-plane (a'') modes are generally much stiffer than the in-plane (a') ones. The tendency means that the out-of-plane perturbation of the external field, which might possibly bring about the $\pi-\sigma$ mixing, is not significant to cause the remarkable enhancement.

3.2.3. Auxiliary Systems−Pyrazine Anion and Deformed Benzene. Two auxiliary systems are examined to corroborate the above conclusion that the conspicuous enhancement of the charge sensitivity of pyrazinyl radical is not simply brought about by the additional contribution of the unpaired radical electron, but by the $\pi-\sigma$ mixing that facilitates the deformation of the π-electron orbitals. The calculation and analysis for the planar pyrazine anion and the deformed nonplanar benzene are crucial to distinguish these two origins. The former species has the unpaired radical electron analogous with that of pyrazinyl radical, but the planar configuration prohibits the $\pi-\sigma$ mixing. The latter species has no radical electron like the stable benzene or pyrazine but allows the $\pi-\sigma$ mixing.

Table 8. Comparison of the Decomposition Analysis of Pyrazine and the Planar Pyrazine Anion (See the Text)

|	py	py⁻ total	α	β	occ. MO
$b_{1u}-b_{3g}$ $(\pi-\pi)$		−12.129	−12.129		unpaired orbital
$b_{2g}-a_u$ $(\pi-\pi)$	−23.97	−25.50	−9.84	−15.66	
$b_{3g}-b_{1u}$ $(\pi-\pi)$	−5.71	−6.08	−1.27	−4.82	
$b_{2u}-a_g$ $(\sigma-\sigma)$	−12.53	−14.72	−7.29	−7.42	lone pair of N
a_g-b_{2u} $(\sigma-\sigma)$	−11.85	−13.37	−6.65	−6.72	lone pair of N
$b_{1u}-b_{3g}$ $(\pi-\pi)$	−7.85	−6.21	−0.45	−5.76	
total	−70.35	−87.94	−42.22	−45.72	
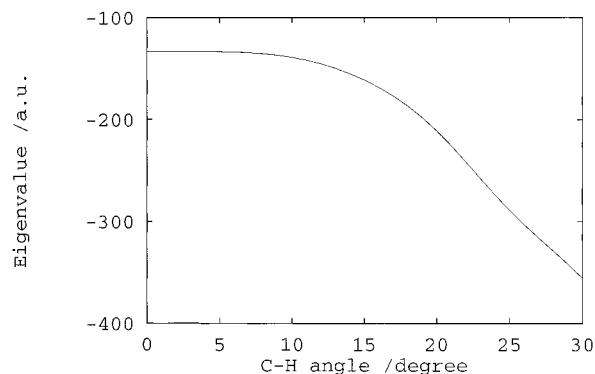
Figure 4. Dependence of the C−H wagging angle of benzene on the first eigenvalue of its response kernel. All the bond lengths are fixed, and only one hydrogen atom of benzene was moved out of the molecular plane. The extended-site model of benzene was employed.

First we give the result of the pyrazine anion in the following. The geometry of the pyrazine anion was taken to be the same as that of the optimized pyrazine (see Figure 1). The total energy was −262.681 922 hartrees via UHF calculation with the DZP basis set.[36] The eigenvalue of the softest normal mode λ_1 was calculated to be −87.94, which is close to that of pyrazine, −70.35, rather than pyrazinyl radical, −294.61. The decomposition using the soft MO pairs revealed that each MO pair except that of the unpaired orbital finds an equivalent pair of pyrazine with the same symmetry and character (see Table 8). Their contribution to λ_1 is listed in Table 8 for comparison. The table demonstrates that a slight enhancement of λ_1 is attributed to the unpaired orbital and that the other equivalent orbital pairs make similar contributions to λ_1.

We then deal with the deformed benzene. The deformation was performed by moving one hydrogen atom while the other atoms remain fixed. The hydrogen atom was moved out of the molecular plane with the C−H bond length fixed to be 1.101 Å, and accordingly, the molecular symmetry became C_s. Figure 4 shows the dependence of the first eigenvalue of the response kernel on the C−H wagging angle. We employed here the extended-site model of the deformed benzene which is analogous with that of pyrazinyl radical. The moderate deformation brought about the significant enhancement of the eigenvalue of the softest normal mode, even if it has no radical electron. We confirmed that the enhancement is attributed mainly to the $\pi-\sigma$ mixing.

These results suggests that the significant enhancement of the charge sensitivity in the aromatic species becomes a considerable factor of the aromatic reactions in solution. Unstable configurations of the aromatic species during a reaction, where the original aromaticity is partly broken due to the attacking reagents, are expected to show the particular softness in the charge redistribution. These states can be particularly sensitive to the perturbation by the surrounding solvent.

3.3. Acetone and 2-Hydroxypropyl Radical. Acetone and 2-hydroxypropyl radical are another pair of parent and radical;
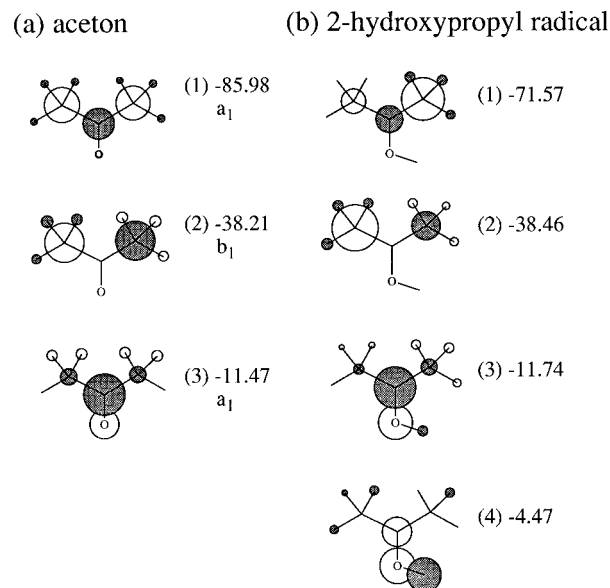
Figure 5. Normal modes and their eigenvalues of the response kernel of (a) acetone and (b) 2-hydroxypropyl radical. See Figure 2.

the latter is formed by the hydrogen abstraction from the former. The calculated effective charges assigned to the atomic sites are listed in Table 4b. When we compare the normal modes of their response kernels in Figure 5, we find that the extra hydrogen does not cause as much difference in the first normal mode as that of pyrazinyl radical. The eigenvalue λ_1 is in fact rather reduced ($\lambda_1 = -85.98 \rightarrow -71.57$), which shows a sharp contrast to the case of pyrazine and pyrazinyl radical. We elucidate the difference with the help of another auxiliary system, β-propyl radical, in the following.

3.3.1. Acetone. As shown in Figure 5, the softest normal mode of both acetone and 2-hydroxypropyl radical is characterized by charge polarization on the C−C and C−H bonds. C−O polarization seems to be too stiff to become a main component of the softest normal mode, but it chiefly constitutes the third normal mode. This suggests that the π electrons on the C−O bond play a less significant role on the charge polarization than the π electrons of pyrazine. The decomposition analysis based on the localized orbitals corroborated the suggestion. Table 9a, the result of acetone, proved that the C−C and C−H σ-bond orbitals govern the softest normal mode of the charge polarization, while the π and n (lone pair) orbitals on the ketyl group C=O influence surprisingly little. Predominance of the hydrocarbon σ-bond orbitals manifests a fundamental feature of this σ-electron system. Among the six C−H σ bonds, the out-of-plane orbitals ($C_3 - H_7$, $C_3 - H_9$, $C_4 - H_8$, $C_4 - H_{10}$) contribute more than the in-plane ones ($C_3 - H_5$, $C_4 - H_6$). The enhancement is ascribed to the hyperconjugation due to the pseudo π character. This effect is emphasized because the central carbon C_1 is of sp² type that facilitates the conjugation.

3.3.2. 2-Hydroxypropyl Radical. The decomposition result of 2-hydroxypropyl radical in Table 9b shows a noticeable difference. The C−C and C−H σ-bond orbitals considerably reduce their contribution while the lone pairs of the oxygen atom become larger. The two factors cancel each other to bring about slight reduction of the total λ_1. The largest factor of reduction is that the augmented contribution of the out-of-plane C−H bond orbitals mentioned above is not observed in the radical. This is because the central carbon C_1 gains sp³ character which is unfavorable for the hyperconjugation. The suppression of the hyperconjugation is quite a substantial consequence of the hydrogen abstraction, but we demonstrate that this effect is not

Table 9. Decomposition of the Softest Normal Mode of (a) Acetone and (b) 2-Hydroxypropyl Radical Based on Their Localized Orbitals

(a) Acetone

−0.001	O_1 core	−8.261	$C_3-H_5\ \sigma$
−0.004	C_2 core	−12.554	$C_3-H_7\ \sigma$
−0.023	C_3 core	−12.554	$C_3-H_9\ \sigma$
−0.023	C_4 core	−8.261	$C_4-H_6\ \sigma$
−0.812	O_1-C_2 banana^a	−12.554	$C_4-H_8\ \sigma$
−0.812	O_1-C_2 banana^a	−12.554	$C_4-H_{10}\ \sigma$
−7.410	C_2-C_3 s	−1.376	O_1 lone pair
−7.410	C_2-C_4 s	−1.376	O_1 lone pair
	total: −85.984		

(b) 2-Hydroxypropyl Radical

α	β	total	
−0.010	−0.010	−0.020	O_1 core
−0.009	−0.002	−0.011	C_2 core
−0.004	−0.004	−0.008	C_3 core
−0.004	−0.004	−0.008	C_4 core
−0.592	−2.215	−2.806	$O_1-C_2\ \sigma$
−1.214	−1.438	−2.651	$C_2-C_3\ \sigma$
−1.340	−1.525	−2.865	$C_2-C_4\ \sigma$
−2.761	−3.091	−5.851	$C_3-H_5\ \sigma$
−2.552	−2.572	−5.124	$C_3-H_7\ \sigma$
−2.692	−2.130	−4.822	$C_3-H_9\ \sigma$
−3.186	−3.369	−6.555	$C_4-H_6\ \sigma$
−4.005	−3.503	−7.508	$C_4-H_8\ \sigma$
−3.448	−3.350	−6.798	$C_4-H_{10}\ \sigma$
−1.972	−2.221	−4.194	$O_1-H_{11}\ \sigma$
−5.061	−8.006	−13.068	$O_1\ \pi$ lone pair
−3.368	−3.008	−6.376	$O_1\ \sigma$ lone pair
−2.901		−2.901	$C_2\ \pi$ (unpaired)
−35.120	−36.447	−71.567	totals

^{a} Hybrid of π and σ orbitals.

Table 10. Decomposition of β-Propyl Radical Based on the Localized Orbitals (Two Geometries, (a) equilibrium and (b) planar, Are Compared)

(a) Equilibrium Geometry

α	β	total	
−0.030	−0.010	−0.040	C_1 core
−0.006	−0.006	−0.012	C_2 core
−0.006	−0.006	−0.012	C_3 core
−2.274	−2.227	−4.501	$C_1-C_2\ \sigma$
−2.274	−2.227	−4.501	$C_1-C_3\ \sigma$
−3.534	−3.823	−7.357	$C_2-H_4\ \sigma$
−4.271	−3.242	−7.513	$C_2-H_6\ \sigma$
−3.739	−3.787	−7.527	$C_2-H_8\ \sigma$
−3.534	−3.823	−7.357	$C_3-H_5\ \sigma$
−4.271	−3.242	−7.513	$C_3-H_7\ \sigma$
−3.739	−3.787	−7.527	$C_3-H_9\ \sigma$
−4.774	−12.541	−17.315	$C_1-H_{10}\ \sigma$
−8.624		−8.624	$C_1\ \pi$ (unpaired)
−41.0783	−38.720	−79.798	totals

(b) Planar Geometry

α	β	total	
−0.000	−0.002	−0.002	C_1 core
−0.000	−0.011	−0.011	C_2 core
−0.000	−0.011	−0.011	C_3 core
−2.666	−3.331	−5.996	$C_1-C_2\ \sigma$
−2.666	−3.331	−5.996	$C_1-C_3\ \sigma$
−4.312	−4.271	−8.583	$C_2-H_4\ \sigma$
−7.290	−6.971	−14.261	$C_2-H_6\ \sigma$
−7.290	−6.971	−14.261	$C_2-H_8\ \sigma$
−4.312	−4.271	−8.583	$C_3-H_5\ \sigma$
−7.290	−6.971	−14.261	$C_3-H_7\ \sigma$
−7.290	−6.971	−14.261	$C_3-H_9\ \sigma$
−0.658	−0.593	−1.251	$C_1-H_{10}\ \sigma$
−0.497		−0.497	$C_1\ \pi$ (unpaired)
−44.270	−43.703	−87.974	totals

restricted to this species. The equivalent effect is also observed in a simpler example, β-propyl radical $CH_3\dot{C}HCH_3$. The wagging motion of the central C−H bond has the identical effect on the hyperconjugation. We thus examine this sample to supplement the above discussion and to clarify the difference between aromatic and nonaromatic species.

3.3.3. Auxiliary System−β-Propyl Radical. We investigated the influence of the wagging distortion of the central H atom (namely H_{10}, see Figure 1c) in contrast with the case of benzene. Two geometries of β-propyl radical were compared: the equilibrium geometry with C_s symmetry and "planar" geometry with C_{2v} where the three carbon atoms and H_{10} lie on a same plane. Both geometries were optimized within the restriction of each symmetry via the UHF calculation with the DZP basis set.[36] The total energy is −117.664 202 hartrees for the equilibrium and −117.663 668 hartrees for the planar, the difference of which is only 0.34 kcal/mol. The equilibrium wagging angle of the central hydrogen is 21.1°. The result of the decomposition analysis based on the localized orbitals is listed in Table 10. The wagging distortion of the C−H bond induces slight reduction of the charge sensitivity of β-propyl radical (−87.974 → −9.798), while that induces significant enhancement of benzene (see Figure 4). The effect of the wagging distortion of β-propyl radical and benzene parallels the effect of the hydrogen abstraction of acetone and pyrazine. The deviation from the planar configuration makes the contribution of the occupied π-electron orbitals ($C_1\ \pi$ and $C_1-H_{10}\ \sigma$ in Table 10) greatly enhanced due to the $\sigma-\pi$ mixing, which is common with the case of benzene. However, there is another important mechanism to reduce the charge sensitivity of β-propyl radical. The deviation from the planarity reduces contribution of the out-of-plane C−H bond orbitals ($C_2 − H_6$,

$C_2 − H_8$, $C_3 − H_7$, $C_3 − H_9$) of the methyl moieties due to the suppression of the hyperconjugation.

We think that the different response of aromatic and non-aromatic species deserves further study. It is noted that β-propyl radical prefers the nonplanar geometry, while benzene prefers the planar geometry. In both cases, however, stable geometry prefers stiff charge polarization. This tendency is consistent with the principle of maximum hardness proposed by Pearson[40] and received intensive examination thereafter,[41−46] although the sensitivity of intramolecular polarization is not identical to the absolute softness which is usually estimated by the inversion of the HOMO−LUMO energy gap.

4. Conclusion

The response kernel $(\partial Q_a/\partial V_b)$ is a site-based expression of the intramolecular charge polarization induced by the external electrostatic field. We defined this quantity in the *ab initio* MO theory and calculated it via the CPHF equations of RHF and UHF wave functions. The result was discussed on the basis of the normal mode analysis. The softest normal mode was further analyzed by the decomposition scheme based on the intrinsic MO pairs or the localized orbitals to examine the distortion of the MO's. In this paper, we particularly studied the effect of

(40) Pearson, R. G. *J. Chem. Educ.* **1987**, *64*, 561.
(41) Pearson, R. G. *Acc. Chem. Res.* **1993**, *26*, 250.
(42) Parr, R. G.; Chattaraj, P. K. *J. Am. Chem. Soc.* **1991**, *113*, 1854.
(43) Chattaraj, P. K.; Nath, S.; Sannigrahi, A. B. *Chem. Phys. Lett.* **1993**, *212*, 223.
(44) Roy, R.; Chandra, A. K.; Pal, S. *J. Phys. Chem.* **1994**, *98*, 10447.
(45) (a) C.-Jiron, G. I.; Lahsen, J.; T.-Labbe, A. *J. Phys. Chem.* **1995**, *99*, 5325. (b) C.-Jiron, G. I.; J.; T.-Labbe, A. *Ibid.* **1995**, *99*, 12730.
(46) Ghanty, T. K.; Ghosh, S. K. *J. Phys. Chem.* **1996**, *100*, 12295.

hydrogen abstraction on the sensitivity of the intramolecular charge polarization.

We found that pyrazine shows remarkable enhancement of the charge sensitivity when it gains an extra hydrogen to form pyrazinyl radical, though the usual polarizability is little altered. The enhancement is largely attributed to the softest normal mode that has alternate amplitude on the ring skeleton. The decomposition analysis revealed that the remarkable enhancement is not simply brought about by the additional contribution of the unpaired radical electron, but the $\pi-\sigma$ mixing that facilitates the deformation of the π-electron orbitals. The same mechanism also greatly augments the charge sensitivity of benzene, another aromatic species, when it is deformed. When one of the C$-$H bonds of benzene is moved out of the molecular plane, the charge sensitivity of the softest normal mode is quite enhanced due to the same mechanism.

We also found, on the other hand, that acetone does not show such enhancement of the charge sensitivity but a slight reduction when it gains an extra hydrogen to form 2-hydroxypropyl radical. In acetone or 2-hydroxypropyl radical, the charge polarization of the softest mode is carried out mainly by the hydrocarbon σ-bond orbitals, not by the π or n orbitals of the ketyl moiety. The hydrogen abstraction diminishes the contribution of the hydrocarbon σ-bond orbitals, especially the hyperconjugation within the hydrocarbon skeleton, which cancel the augmented contribution of the π and n orbitals of the ketyl group. The same mechanism is also observed in the effect of the wagging motion of the central C$-$H bond of β-propyl radical. The deviation from the planar structure suppresses the hyperconjugation, which works to reduce the charge sensitivity of this σ-electron system.

Finally, we make a brief remark on the further study. The remarkably different response of aromatic and nonaromatic species seems to be a rather general phenomenon. We expect that the difference has to be elucidated from the stability of aromaticity, since the aromaticity is well evaluated with the hardness.[47] As we mentioned in section 1, such aromatic radicals as pyrazinyl radical or benzophenone ketyl radical show anomalously slow diffusion in solution. We already have preliminary evidence that the anomaly is derived from the significant enhancement of the charge sensitivity. We will describe the results in a future paper.

(47) (a) Zhou, Z.; Parr, R. G.; Garst, J. F. *Tetrahedron Lett.* **1988**, *29*, 4843. (b) Zhou, Z.; Parr, R. G. *J. Am. Chem. Soc.* **1989**, *111*, 7371.